# Core Flow Modelling Assumptions

Ciarán Beggan, Kathy Whaler

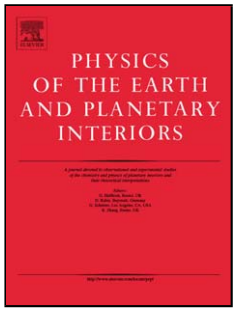


Title: Core Flow Modelling Assumptions

Authors: Ciarán Beggan, Kathy Whaler

PII: S0031-9201(08)00081-2
DOI: doi:10.1016/j.pepi.2008.04.011
Reference: PEPI 4932

To appear in: *Physics of the Earth and Planetary Interiors*

Received date: 15-10-2007
Revised date: 21-4-2008
Accepted date: 23-4-2008

Please cite this article as: Beggan, C., Whaler, K., Core Flow Modelling Assumptions, *Physics of the Earth and Planetary Interiors* (2007), doi:10.1016/j.pepi.2008.04.011

# Core Flow Modelling Assumptions

Ciarán Beggan * , Kathy Whaler

*School of GeoSciences, University of Edinburgh, Edinburgh EH9 3JW, UK*

**Abstract**

Modelling of core flows at the core-mantle boundary from secular variation requires a range of both physical and mathematical assumptions in order to derive a solution. We investigate the role of certain assumptions and an $L_1$ norm iterative inversion method to derive core flow models. Using three datasets of secular variation, we separate the effects of: *(a)* the assignment of observation errors through the data covariance matrix, *(b)* the *a priori* constraints placed upon the solution and *(c)* the type of flow regime assumed to be present in the core. Flow is calculated directly from the time derivatives of the $X$, $Y$ and $Z$ components of ground-based observatories rather than Gauss coefficients of the secular variation. We find the $L_1$ iterative method improves the fit of the secular variation generated by the flow models to the observed data, compared to the $L_2$ norm (least-squares) method. Using this method, we find a new class of flow solutions explaining the secular variation: purely poloidal flows, which fit the input data adequately, and, for one of our datasets, better than toroidal-only flows. The patterns of motions is very different from that seen in previous flow models, which are dominated by their toroidal component.

*Key words:* Core Flow, Geomagnetic Field, Regularisation, Secular Variation

## 1 Introduction

The Earth's main magnetic field is generally accepted to be generated and sustained by dynamo action associated with the motion of the electrically conducting fluid outer core. The main field evolves slowly over time; the gradual decadal timescale change of the main field is known as the secular variation (SV). Whether and how the evolution of the field over these timescales can be used to constrain the nature of the fluid motion has been a matter of on-going research for several decades. Work by Roberts and Scott (1965) formulated the problem of determining flow along the core-mantle boundary from measurements of SV, which was implemented by e.g. Kahle et al. (1967).

Under the main assumption, termed the frozen-flux approximation, that the SV of the main field is due to the simple advection of the field lines through fluid motion, disregarding any effects of diffusion (Roberts and Scott, 1965). The neglect of diffusion is justified by examining the behaviour of the field at large horizontal scales over short time intervals. However, there are shortcomings to this assumption which are discussed in, for example, Gubbins and Kelly (1996), Braginsky and LeMouël (1993) and Love (1999). Furthermore, even under the frozen-flux assumption, deducing the flow velocity from the field and SV cannot be achieved uniquely, as there are entire classes of flow which do not generate any detectable SV outside the core (Backus, 1968). Therefore, further assumptions are made about the type of flow at the core-mantle boundary (CMB), to reduce the inherent non-uniqueness. Examples of non-uniqueness reducing assumptions include steady flows (Voorhies and

* Corresponding author.
*Email address:* ciaran.beggan@ed.ac.uk (Ciarán Beggan).

Backus, 1985), toroidal-only (Whaler, 1980), tangentially geostrophic (Hills, 1979; Le Mouël, 1984) or flows with a particular helicity (Amit and Olson, 2004). Further assumptions must be made to produce a tractable problem, since only a finite quantity of inaccurate data is available. In particular, the flow is truncated at a large scale and a regularised solution is calculated via a damping (smoothing) parameter.

We wish to examine the role that underlying assumptions can have on the resulting core flow models. The past decade has seen a vast improvement in the global quality and quantity of data from satellite measurements. However, in this study we employ data from ground-based observatories, in order to calculate directly observed SV. This allows us to disregard any concern about how to account for the temporal discontinuity in satellite data for any particular point on the Earth's surface. Contamination from sources external to the observatory at ground level are well understood. At satellite altitudes, these sources can be internal (as well as external) to the orbit, complicating their removal. In contrast to most other studies, we invert SV calculated from observatory data – rather than spherical harmonic model coefficients – to compute flow model coefficients. This allows a more rigorous test of flow assumptions made, and incorporation of realistic data uncertainties.

This paper examines the results of comparisons between combined and toroidal-only flows to model the observed SV, using a one-norm minimisation inversion technique, initially imposing a minimum global root-mean-square (RMS) flow velocity constraint. Poloidal-only flows were also examined, for completeness, throwing up a number of interesting results which we will elucidate upon below. Further, we highlight the competing effects of the various assumptions to control the final flow model.

## 2 Method

The inverse problem of deriving a CMB flow model from observed SV data is typically approached through relating spherical harmonic representations of the Main Field, SV, and flow (e.g. Kahle et al., 1967; Whaler, 2007). As the horizontal velocity averages to zero over the CMB with the radial component across the boundary vanishing, the flow can be expressed in terms of poloidal ($s$) and toroidal ($t$) scalars that can be expanded in spherical harmonics. Their coefficients, stored in a vector $\mathbf{m}$, are the flow model coefficients whose values we seek using a regularised inversion approach.

Spherical harmonic SV coefficients ordered in a vector ($\dot{\mathbf{g}}$) are related to flow coefficients by $\dot{\mathbf{g}} = \mathbf{Bm}$ where the elements of $\mathbf{B}$ are linear combinations of Elsasser and Gaunt integrals, whose multipliers depend on the main field coefficients. The vector $\dot{\mathbf{g}}$ is related to the SV data on the surface of the Earth by $\mathbf{d} = \mathbf{Y}\dot{\mathbf{g}}$. Here, the elements of the data vector, $\mathbf{d}$, are the observed SV components (e.g. $\dot{X}$, $\dot{Y}$ and $\dot{Z}$, where $X$, $Y$ and $Z$ denote the North, East and vertically downwards respectively) expressed in spherical polar coordinates. $\mathbf{Y}$ has elements which are multiples of spherical harmonics and their $\theta$ and $\phi$ derivatives. Thus, including the observational error ($\mathbf{e}$), the linear inverse problem becomes:

$$\mathbf{d} = \mathbf{Y}\dot{\mathbf{g}} + \mathbf{e} = \mathbf{YBm} + \mathbf{e} = \mathbf{Am} + \mathbf{e} \tag{1}$$

We determine a model by regularised inversion, minimising an objective function combining the size, or norm, of the error vector (the error norm), and a measure of 'complexity' or 'smoothness' of the solution (the solution norm). We use both the $L_1$ (or Laplacian) norm, which minimises the absolute sum of

the errors, and the standard $L_2$ least-squares formulation. Errors in the measurements can often be correlated, so a data covariance matrix (denoted $\mathbf{C}_e$), where the diagonal elements are the variances of the data, is used to capture this information.

$L_2$ minimisation gives

$$\hat{\mathbf{m}} = (\mathbf{A}^T\mathbf{C}_e^{-1}\mathbf{A} + \lambda\mathbf{D})^{-1}\mathbf{A}^T\mathbf{C}_e^{-1}\mathbf{d} \tag{2}$$

where $\mathbf{D}$ is the regularisation matrix which is used to impose 'smoothness'. A damping parameter, $\lambda$, acts to control the importance attached to fitting the data versus the imposition of a smooth solution. Regularisation also ensures numerical stability of the inversion and convergence when the spherical harmonic series for $\mathbf{m}$ is truncated. In this study, the flow vector $\mathbf{m}$, the main field model $\mathbf{g}$ and the intermediate SV model $\dot{\mathbf{g}}$ are truncated at degree $l = 14$.

Walker and Jackson (2000) provide the motivation to calculate the model by an iterative one-norm minimisation method instead. In particular, they offer empirical evidence that the distribution of residuals from a historical magnetic dataset comprising vector, scalar and directional data is well-described by a double-Laplacian probability distribution. Note that Walker and Jackson (2000) modelled the magnetic field itself, rather than CMB flow, with data being main field rather than SV observations. Here, we examine whether the same is true of the distribution of SV residuals.

We use Walker and Jackson's (2000) implementation of the one-norm solution. The residual errors from the previous iteration are used to specify an additional diagonal matrix $\mathbf{R}$, whose elements are $R_{ii} = \sqrt{2}/|e_i|$, where $e_i$ is the residual of the $i$th datum. $\mathbf{R}$ is recalculated at each iteration, hence the data are

iteratively re-weighted, reducing the influence of outliers. Relabelling $\mathbf{C}_e^{-1}$ as $\mathbf{E}$ (to maintain consistency with the notation used in Walker and Jackson (2000)), the iterative regularised one-norm solution can be written as:

$$\hat{\mathbf{m}}_{i+1} = (\mathbf{A}^T\mathbf{E}^T\mathbf{R}\mathbf{E}\mathbf{A} + \lambda\mathbf{D})^{-1}(\mathbf{A}^T\mathbf{E}^T\mathbf{R}\mathbf{E}\ \mathbf{d}) \tag{3}$$

In this study, two formulations of $\mathbf{D}$ are used, both of which measure quadratic norms of the flow. The 'strong velocity norm' of Bloxham (1988) is a global measure of the flow complexity, whose square is

$$\begin{aligned}\mathbf{m}^T\mathbf{Q}\mathbf{m} &= \oint_{CMB} \left[\left(\nabla_h^2 u_\theta\right)^2 + \left(\nabla_h^2 u_\phi\right)^2\right] dS \\ &= 4\pi \sum_l \frac{[l(l+1)]^3}{2l+1} \sum_{m=0}^{l} [(t_l^m)^2 + (s_l^m)^2]\end{aligned} \tag{4}$$

where $u_\theta$ and $u_\phi$ are the horizontal flow components.

An alternative is to minimise the CMB RMS SV. This is typically applied when undertaking regularised inversion for SV coefficients (Gubbins, 1983), but can also be used for flow modelling (Whaler, 1986). It imposes smoothness on the SV predicted by the flow rather than the flow itself. Let $a$ be the Earth's radius, $c$ the radius of the CMB, and with $\{\dot{g}_l^m, \dot{h}_l^m\}$ the Gauss coefficients of the SV, the square of this solution norm can be defined as:

$$\begin{aligned}\dot{\mathbf{g}}^T\dot{\mathbf{Q}}\dot{\mathbf{g}} &= \mathbf{m}^T\mathbf{B}^T\mathbf{B}\mathbf{m} \\ &= \oint_{CMB} \dot{B}_r^2 d\Omega = 4\pi \sum_l \left(\frac{a}{c}\right)^{2l+4} \frac{(l+2)^2}{2l+1} \\ &\quad \times \sum_{m=0}^{l} (\dot{g}_l^m + \dot{h}_l^m)^2\end{aligned} \tag{5}$$

Equations (4) and (5) can be combined or used separately as required – $\mathbf{Q}$ or

$\mathbf{B}^T\mathbf{B}$ replace $\mathbf{D}$ in (3), e.g. $\mathbf{D}$ is diagonal with elements $l(l+3)^3/(2l+1)$ for (4).

The 'fit' of the flow models to the observed data can be measured via the one-norm ($L_1$) and two-norm ($L_2$) measures of the error residuals defined (where $i$ is the number of observations) as:

$$L_1 = \sum_{i=1}^{N} |e_i| \quad \text{and} \quad L_2 = \sqrt{\sum_{i=1}^{N} (e_i)^2} \tag{6}$$

It is important also to test whether the residuals conform better to a Gaussian or double-Laplacian distribution.

## 3 Observatory Data

Three separate SV datasets were considered, all consisting of $\dot{X}$, $\dot{Y}$ and $\dot{Z}$ data. The initial dataset, termed Dataset 1, was derived from annual means recorded at 172 ground-based observatories for the year 1990. The SV is estimated over 12 months from July 1989 to June 1990. This assumes that there is little or no secular acceleration relative to the size of the SV. Observation errors were assigned to be a nominal 1 $nT/yr$ for all stations and components. The second dataset, termed Dataset 2, consisted of SV calcuated by the same method as Dataset 1, in this case from 176 ground-based observatories, but with a further correction applied to remove internal covariance within the data (Wardinski and Holme, 2006). The associated observation error for each component was estimated by fitting a magnetic field model through a time series of data from 1980–2000 and estimating the covariance of misfit to the model for each direction. The errors ranged from 0.91 to 103 $nT/yr$ for the $X$ direction, with

a median value of 3.8 $nT/yr$. The $Z$ direction was similarly distributed, while the $Y$ direction had the smallest range of values. (The $X$ and $Z$ components are often inversely correlated, due to external field contamination.)

As ground-based observatories are unevenly geographically distributed, a third 'global' synthetic SV data set, consisting of 288 points on the globe separated by 15 ° intervals in latitude and longitude, was created. Dataset 3 was generated from the IGRF10 spherical harmonic model for the epoch 1990.0. The associated observation errors for Dataset 3 were also fixed at a nominal 1 $nT/yr$.

The GUFM1 field model (Jackson et al., 2000) provided the main field coefficients for the Gaunt and Elsasser (i.e. $\mathbf{B}$) matrices. Calculating toroidal- or poloidal-only flow models requires omission of either the Elsasser or Gaunt matrix in the formulation of $\mathbf{B}$ and solving for the desired toroidal or poloidal coefficients respectively. The residual errors for the first iteration of the one-norm solution are obtained from an initial starting model calculated from a $L_2$ solution of the input data. The value of very small ($< 10^{-4}$) error residuals in the matrix $\mathbf{R}$ are set to $10^{-4}$ to prevent the formation of ill-conditioned matrices, as advocated by Walker and Jackson (2000). No other nonuniqueness constraints were imposed on the solution. In common with Walker and Jackson (2000), 15-20 iterations were typically sufficient to ensure solution convergence. We find that the use of this $L_1$ iterative method vastly improves the fit of the model to the data (using the measures in Equation 6 and the distribution of the residuals) compared to $L_2$ minimisation, justifying the use of this approach.

## 4 Comparison of Combined, Toroidal-only and Poloidal-only Flow Models

It has been recognised that toroidal-only flow models can often fit the data adequately, though overall they do not fit well enough (Whaler, 1986). A small poloidal component in the flow increases the number of degrees of freedom, but makes a statistically significant improvement to the data fit. Typically, the ratio of the energy of the toroidal to poloidal flow within a combined (i.e toroidal and poloidal) flow regime averages at approximately 0.85, under the model assumptions from Section 2. An analysis of the individual contribution of each flow coefficient shows that, though most of the flow energy is in the toroidal coefficients, part of it is in the low degree and order coefficients of the poloidal flow, even though overall the total poloidal flow contribution is relatively small.

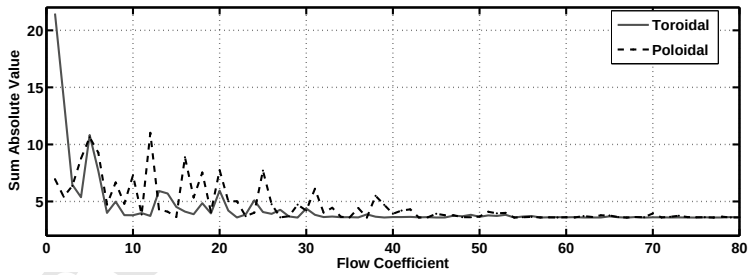


Fig. 1. The sum of the absolute values (SAV) of the residual when each coefficient indicated is not included in the toroidal-poloidal flow solution from Dataset 3. When all 448 coefficients are present, the SAV is 3.59. Coefficients are ordered $t_1^0$, $t_1^{1c}$, $t_1^{1s}$, $t_2^0$, $t_2^{1c}$, etc.

Figure 1 shows the sum of the absolute values (SAV) of the residual errors from a one-norm solution in which an individual flow coefficient has been removed and the resulting difference between the forward model and the ob-

served data is calculated. Coefficients are ordered $t_1^0$, $t_1^{1c}$, $t_1^{1s}$, $t_2^0$, $t_2^{1c}$, etc, with the superscripts $c$ and $s$ denoting coefficients multiplying $\cos m\phi$ and $\sin m\phi$ respectively. With all 448 flow coefficients present, the SAV is 3.59. A higher value thus indicates a worse fit to the data. It can be seen from Figure 1 that excluding individual coefficients lower than degree and order 7 has the largest effect on the solution, demonstrating that the flow has converged above degree and order 8, and that some of the low degree and order poloidal terms contribute significantly to the data fit. For example, solutions without $s_3^{1c}$ (poloidal coefficient 12) fit worse than solutions without $t_2^0$ (toroidal coefficient 4). This observation motivated the comparison of three different flow types (i.e. combined, toroidal- and poloidal-only).

### *4.1 Minimisation using the 'Strong' Velocity Norm*

The results from experiments where the regularising constraint is the minimisation of the 'strong' velocity norm (Equation (4)) are summarised in Table 1. The solution norm (the square root of Equation (4)) of all the models has been set to $2.6 \times 10^5$ $(km/yr)^2$, by appropriate adjustment of the damping parameter ($\lambda$). This corresponds to equalising the 'roughness' of the combined, toroidal- and poloidal-only flows for each dataset, making the three flow regimes directly comparable. This value of the solution norm was chosen to produce a flow model with a 'reasonable' RMS velocity of approximately 16 $km/yr$ for the combined toroidal-poloidal models.

The results from Dataset 1 indicate that the combined flow model has a far better fit to the observatory data than the toroidal-only or poloidal-only models. Surprisingly, the poloidal-only flow model fits the data better than the

toroidal-only model (that is, the one-norm measure of error is smaller). For Datasets 2 and 3, the toroidal-only flow model fits the observations better than the poloidal-only model, but not by a large amount.

The average data misfit (defined as $\sum |e_i|/N$) for both Datasets 1 and 3 is approximately 10 $nT/yr$. The combined flow model produced from Dataset 2 has the lowest spread of residuals, thus giving the best overall fit. The average data misfit for Dataset 2 is 1.1 $nT/yr$. It is interesting to note that, despite the slower RMS flow velocities, poloidal-only models produce an adequate fit to the input SV data.

Figure 2 illustrates the three different flow models calculated from Dataset 2. The accompanying histograms show the residual errors i.e. the difference between the flow model prediction of the SV at each observatory and the actual data recorded. From inspection of Table 1, it appears that the toroidal-only flow and the poloidal-only flow maintain an equally good fit to the observatory data, based on the one-norm and two-norm measures. However, comparison of the histograms of Figure 2 *(e)* and *(f)* indicates that the poloidal-only flow model is actually more strongly peaked about zero than the toroidal flow model. On the other hand, the poloidal-only model has a larger spread of residual values leading to heavier tails than the toroidal-only flow model residuals. The flow patterns of the toroidal-only flow model are broadly similar to the combined model whilst the poloidal-only model has few visible similarities to the full combined model or the poloidal part of the combined flow.

Analysis of the geographical distribution of the residual errors for the flows reveals that the largest deviations occur in the $\dot{X}$ component of the observatory data, concentrated in the northern regions of Asia and Europe.

| Dataset | Model | One-Norm | Two-Norm | Misfit | RMS Vel. |
|---|---|---|---|---|---|
| 1 | TorPol | 4099 | 615 | 7.9 | 15.8 |
| | Tor | 6189 | 658 | 12 | 14.1 |
| | Pol | 6012 | 684 | 11.6 | 7.7 |
| 2 | TorPol | 366 | 30 | 0.7 | 16.6 |
| | Tor | 674 | 49 | 1.3 | 14.3 |
| | Pol | 695 | 58 | 1.3 | 7.9 |
| 3 | TorPol | 3108 | 199 | 3.6 | 15.5 |
| | Tor | 7792 | 406 | 9 | 13.3 |
| | Pol | 8600 | 499 | 9.9 | 7.5 |

Table 1

Fit of flow models to observatory SV data minimising the 'strong' velocity norm. The solution norm of each model is $2.6 \times 10^5 (km/yr)^2$. One-Norm, Two-Norm and Misfit are in $nT/yr$. RMS Velocity is in units of $km/yr$.

### *4.2 Minimisation using the Root Mean Square SV Norm*

The second set of experiments applied the regularising constraint of minimising the CMB RMS SV predicted by the model solutions. Due to numerical instability, minimisation using this norm (Equation (5)) cannot be undertaken directly. Following Whaler (1986) we added a flow constraint, with a very small damping parameter, $\mu$, typically two orders of magnitude smaller than the SV constraint damping parameter. The flow models from the three datasets were

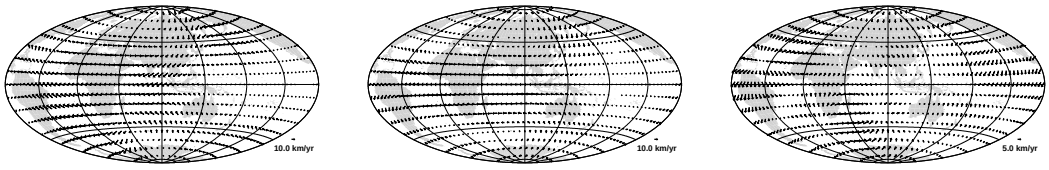


(a) Toroidal-Poloidal Flow Model (b) Toroidal Flow Model (c) Poloidal Flow Model

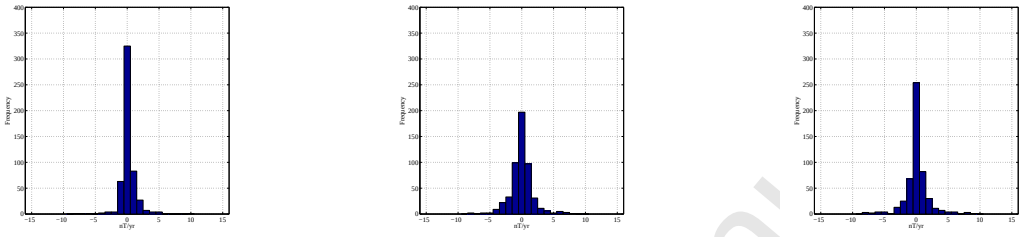


(d) Histogram of Flow Model Data Residuals (e) Histogram of Flow Model Data Residuals (f) Histogram of Flow Model Data Residuals

Fig. 2. Core-mantle boundary flow Models and Histograms of the residuals to the observatory SV data for Dataset 2 with the 'strong' velocity norm applied. Continents shown for reference.

solved in the same manner as previously, altering the values of $\mu$ and $\lambda$ until the 'strong' velocity norms are equal. Table 2 summarises the results. The velocity norm has to be set to a much higher value of $5.8 \times 10^6$ $(km/yr)^2$ to achieve a RMS velocity of approximately 16 $km/yr$ (for the combined flow). With this value, the one-norm and two-norm misfit and RMS velocity metrics of the solutions from the combined flows are comparable to those in Table 1. The toroidal-only and poloidal-only flows are, however, significantly poorer than the solutions calculated with only the 'strong' velocity norm constraint. Furthermore, the flow patterns and residual distributions (Figure 3) reveal that the solutions are markedly different from those in Figure 2.

The effects of increased damping via $\mu$ and $\lambda$ to set the strong velocity norm

equal to $2.6 \times 10^5$ $(km/yr)^2$ (i.e. comparable to the value in Table 1) are shown in Table 3. Extremely poorly fitting solutions are produced, compared to both Tables 1 and 2. The flows minimising the 'strong' velocity norm converge around degree 8. In contrast, the toroidal- and poloiadal-only flow models generated from the RMS SV constraint have no significant power in any particularly dominant degree (their spectra are almost flat), whilst the combined models have some power in the lower degrees, but do not converge until degree 12.

The last column in Tables 2 and 3 gives the RMS SV generated on the CMB for each model. Magnetic field models such as IGRF10 (Macmillan and Maus, 2005) and CHAOS (Olsen et al., 2006) predict values in the range $60 - 70 \times 10^6$ $(nT/yr)^2$. The models in Table 1 behave in a similar manner, generating SV values between 63 and $200 \times 10^6$ $(nT/yr)^2$. As can be seen in Table 2, combined flows generate only slightly higher SV than this for a similar RMS velocity. In contrast, the SV generated by toroidal- and poloidal-only flows is minuscule. For the models in Table 3, the SV generated is orders of magnitude smaller. This is due to the extremely slow flow velocities, reflecting the fact that the models are not vigorous enough to fit the data well, even though they are complex (as reflected by their strong velocity norm value).

Allowing the toroidal- or poloidal-only models in Tables 2 and 3 to become more realistic (by reducing the damping parameters) does generate SV values similar to the standard magnetic field models, but at the cost of greatly increased complexity of the flow. Thus, when using the RMS SV norm, simple flows fit the data poorly, while very complex flows are needed to generate a realistic amount of CMB SV and improve the fit to observations.

| Dataset | Model | One-Norm | Two-Norm | Misfit | RMS Vel. | RMS SV |
|---|---|---|---|---|---|---|
| 1 | Tor+Pol | 3925 | 195 | 7.6 | 15.3 | 239 |
| | Tor | 11966 | 882 | 23 | 5.1 | 0.08 |
| | Pol | 11519 | 865 | 22.3 | 5.3 | 0.1 |
| 2 | Tor+Pol | 343 | 29 | 0.6 | 16.0 | 268 |
| | Tor | 1628 | 112 | 3.1 | 5.1 | 0.07 |
| | Pol | 1618 | 111 | 3.1 | 5.3 | 0.1 |
| 3 | Tor+Pol | 2861 | 200 | 3.3 | 15.6 | 118 |
| | Tor | 18132 | 886 | 20.9 | 5.6 | 0.3 |
| | Pol | 17923 | 883 | 20.7 | 5.8 | 0.05 |

Table 2

Fit of flow models to observatory SV data minimising the Root-Mean-Square Secular Variation over the CMB. The 'strong' velocity norm value of each model is $5.8 \times 10^6 (km/yr)^2$. RMS CMB SV is in units of $10^6$ $(nT/yr)^2$. Other units as for Table 1.

## 5 Discussion

In this study we find a number of new results. Firstly, the allocation of the error budget through the covariance matrix has a dramatic effect on the fit of the flow to the observations. The observation errors for Datasets 1 and 3 have been set equal; a simple but physically unrealistic allocation. In contrast, the observation errors in Dataset 2, have been corrected for covariance between the $X$, $Y$ and $Z$ observatory components, to improve the removal of exter-

| Dataset | Model | One-Norm | Two-Norm | Misfit | RMS Vel. | RMS SV |
|---|---|---|---|---|---|---|
| 1 | Tor+Pol | 7632 | 722 | 14.8 | 3.9 | 1.4 |
| | Tor | 13811 | 955 | 26.8 | 1.1 | 0.0005 |
| | Pol | 13859 | 957 | 26.9 | 1.1 | 0.0003 |
| 2 | Tor+Pol | 971 | 75 | 1.8 | 3.9 | 1.4 |
| | Tor | 1808 | 121 | 3.4 | 1.2 | 0.02 |
| | Pol | 1824 | 122 | 3.5 | 1.2 | 0.02 |
| 3 | Tor+Pol | 15363 | 761 | 17.8 | 3.3 | 0.5 |
| | Tor | 23690 | 1123 | 27.4 | 1.0 | 0.003 |
| | Pol | 23478 | 1114 | 27.2 | 1.1 | 0.004 |

Table 3

Fit of flow models to observatory SV data minimising the Root-Mean-Square Secular Variation over the CMB. The 'strong' velocity norm value has been matched to that of Table 1. Units as in earlier tables.

nal field contamination. Including additional information about data quality through the covariance matrix leads to an improved fit. Tables 1 and 2, and the histograms of residuals, indicate that Dataset 2 consistently achieves the flow with the best fit to the SV input data.

Secondly, the choice of solution norm alters the resultant flow pattern significantly, despite an equivalently good fit. Minimisation using the 'strong' velocity norm (Figure 2) produces flows showing patterns similar to those of other studies (e.g. Bloxham and Jackson, 1991; Waddington et al., 1995;

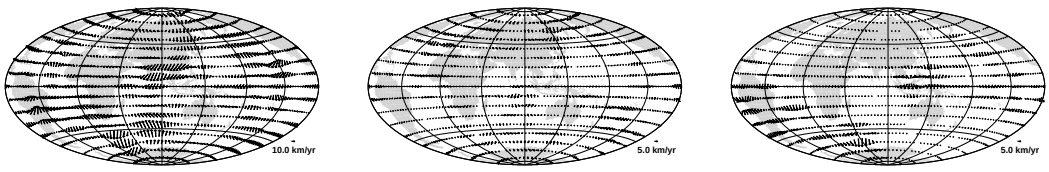


(a) Toroidal-Poloidal Flow Model (b) Toroidal Flow Model (c) Poloidal Flow Model

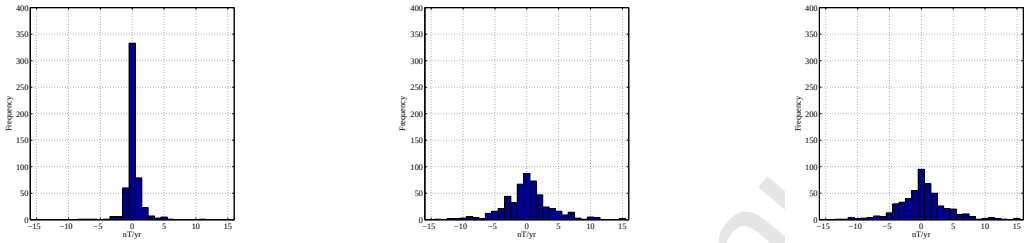


(d) Histogram of Flow Model Data Residuals (e) Histogram of Flow Model Data Residuals (f) Histogram of Flow Model Data Residuals

Fig. 3. Flow Models and Histograms of the residuals to the observatory SV data for Dataset 2 minimising the RMS SV predicted by the flow. Note the contrast with Figure 2.

Holme and Olsen, 2006). However, the flows resulting from minimising CMB root-mean-square $SV$ are more complex (Figure 3) and admit only combined flow model solutions. They do not match the typical patterns found in other core flow studies.

Thirdly, the existence of seemingly viable and relatively well-fitting poloidal-only flow models is a surprising result (Figure 2), given that such flows are currently considered physically unfeasible in the core dynamic regime. Note that Dataset 3 consists of evenly geographically distributed 'stations', indicating that the conclusions drawn here are not a function of the particular distribution of observatories available.

Love (1999) developed a dynamo model in which poloidal-only flow dominates at the CMB. That particular dynamo model exhibited no SV at the surface, but does illustrate that such flows are theoretically possible. In contrast, our poloidal-only flows generate sufficient SV to explain the observations. However, Gubbins (2007) shows that strong poloidal flows would expel large amounts of toroidal flux from the core, thus undermining the frozen-flux hypothesis on which flow inversion is predicated. Our poloidal flows may be sufficiently weak to overcome this problem.

Combining these previous results with the findings from this study suggests that poloidal-only flows do not provide a good representation of the CMB flow, despite the relatively good fit to the SV data. Additionally, this work shows that CMB SV values matching those in standard models can be easily achieved with velocity norm regularised solutions. In contrast, SV norm regularised solutions produce complex flows for a comparable fit to the data with only slightly smoother CMB SV. Thus solutions minimising the SV norm have no real advantage over those with smooth flows.

## 6 Conclusions

We have employed an $L_1$ error norm iterative minimisation method to invert SV data directly for core flow models. We find this approach improves the fit of the SV generated by the models to the observed data compared to the usual $L_2$ (least-squares) norm. Using SV data rather than spherical harmonic SV models allows us to examine better the effects of some flow assumptions and constraints imposed upon inversions. Using two datasets of SV derived from ground-based observatories and a third consisting of synthetic SV on a

regular grid, it is shown that observation errors affect the overall fit of the flow model to the input data. In particular, using a dataset for which variable observation errors have been calculated for each component by co-estimation improves the overall fit (compared to models obtained assuming equal data errors).

The constraints normally imposed in a regularised inversion are also shown to influence greatly the resultant flow regime. A constraint which minimises a velocity norm of the flow is weaker (i.e. permits a 'larger' model space) than a constraint that minimises the CMB RMS SV predicted by the flow. The weaker constraint allows solutions such as poloidal-only flow models to exist which are equally as valid as toroidal-only flow models, in some cases producing a better fit to the input data. The stronger constraint produces complex flow regimes, which do not match the simpler flow patterns from the weaker constraint or results from other studies. Therefore, it probably has little use beyond hypotheses testing frozen-flux and flow modelling assumptions. We therefore recommend CMB flows are derived by the $L_1$ norm minimisation method with a velocity norm constraint.

## Acknowledgements

We would like to thank Ingo Wardinski for sharing the covariance corrected secular variation dataset. We also thank Richard Holme and Andrew Jackson for useful discussion of this work and Susan Macmillan for constructive comments on the manuscript. Part of this work was presented at a meeting organised by Keke Zhang to celebrate the 60th birthday of David Gubbins, one of the pioneers of modern geomagnetism. We thank David Gubbins for helpful com-

ments on an earlier version of this manuscript. KAW acknowledges his advice, encouragement and support throughout her career. This research is part of the NERC GEOSPACE programme, funded under grant NER/O/S/2003/00674. CDB is funded under NERC studentship award NER/S/J/2005/13496.

## References

Amit, H., Olson, P., 2004. Helical core flow from geomagnetic secular variation. Phys. Earth Planet. Int. 147, 1–25.

Backus, G. E., 1968. Kinematics of geomagnetic secular variation in a perfectly conducting core. Philos. Trans. R. Soc. Lond. Ser A 263, 239–266.

Bloxham, J., 1988. The determination of fluid flow at the core surface from geomagnetic observations. Vol. Mathematical Geophysics. D. Reidel Publishing Company, Ch. 9, pp. 189–208.

Bloxham, J., Jackson, A., February 1991. Fluid flow near the surface of Earth's outer core. Reviews of Geophysics 29, 1, 97–120.

Braginsky, S., LeMouël, 1993. Two-scale model of a geomagnetic field variation. Geophys. J. Int. 112, 147–158.

Gubbins, D., 1983. Geomagnetic field analysis - I. Stochastic inversion. Geophys. J. R. Astr. Soc. 73 (3), 641–652.

Gubbins, D., 2007. Geomagnetic constraints on stratification at the top of the Earth's core. Earth Planets Space 59, 661–664.

Gubbins, D., Kelly, P., 1996. A difficulty with using the frozen flux hypothesis to find steady core motions. Geophys. Res. Lett. 23 (14), 1825–1828.

Hills, R., 1979. Convection in the eath's mantle due to viscous shear at the core-mantle interface and due to large-scale bouyancy. Ph.D. thesis, N.M. State Univ., Las Cruces.

366 Holme, R., Olsen, N., 2006. Core surface flow modelling from high-resolution
367 secular variation. Geophys. J. Int. 166, 518–528.
368 Jackson, A., Jonkers, A., Walker, M., 2000. Four centuries of geomagnetic secu-
369 lar variation from historical records. Philos. Trans. R. Soc. Lond. 358 (1768),
370 957–990.
371 Kahle, A., Vestine, E., Ball, R., 1967. Estimated surface motions of the Earth's
372 core. J. Geophys. Res. 72, 1095–1108.
373 Le Mouël, J., 1984. Outer-core geostrophic flow and secular variation of Earth's
374 geomagnetic field. Nature 311, 734 – 735.
375 Love, J., 1999. A critique of frozen-flux inverse modelling of a nearly steady
376 geodynamo. Geophys. J. Int. 138, 353–365.
377 Macmillan, S., Maus, S., 2005. International geomagnetic reference field:the
378 tenth generation. Earth Planets Space 57, 1135–1140.
379 Olsen, N., Luhr, H., Sabaka, T., Mandea, M., Rother, M., Toffner-Clausen,
380 L. a., 2006. Chaos: a model of the earth's magnetic field derived from champ,
381 rsted, and sac-c magnetic satellite data. Geophys. J. Int. 166, 67–75.
382 Roberts, P., Scott, S., 1965. On the analysis of the secular variation. 1. A
383 hydromagnetic constraint: Theory. J. Geomag. Geoelec. 17, 137–151.
384 Voorhies, C., Backus, G., 1985. Steady flows at the top of the core from ge-
385 omagnetic field models: The steady motion theorem. Geophys. Astrophys.
386 Fluid Dynam. 32, 163–173.
387 Waddington, R., Gubbins, D., Barber, N., 1995. Geomagnetic field analysis -
388 V. Determining steady core-surface flows directly from geomagnetic obser-
389 vations. Geophys. J. Int. 122 (1), 326–350.
390 Walker, M., Jackson, A., 2000. Robust modelling of the Earth's magnetic field.
391 Geophys. J. Int. 143-3, 799–808.
392 Wardinski, I., Holme, R., 2006. A time-dependent model of the earth's mag-

netic field and its secular variation for the period 1980-2000. J. Geophys. Res. 111, B12101.

Whaler, K., 1980. Does the whole of the Earth's core convect? Nature 287, 528–530.

Whaler, K. A., 1986. Geomagnetic evidence for fluid upwelling at the core-mantle boundary. Geophys. J. R. Astr. Soc. 86, 563–588.

Whaler, K. A., 2007. Encyclopedia of Geomagnetism and Paleomagnetism. Springer, Dordrecht, Ch. Core Motions, pp. 84–89.